ApJ, in press

Light Curves of Rapidly Rotating Neutron Stars

Timothy M. Braje and Roger W. Romani

Dept. of Physics, Stanford University, Stanford, CA 94305-4060

timb@astro.stanford.edu; rwr@astro.stanford.edu

and

Kevin P. Rauch

Dept. of Astronomy, University of Maryland, College Park, MD 20742-2421

rauch@astro.umd.edu

ABSTRACT

We consider the effect of rapid rotation on the light curves of neutron stars with hot polar caps. For $P \approx 3$ms spin periods, the pulse fractions can be as much as an order of magnitude larger than with simple slowly-rotating (Schwarzschild) estimates. Doppler boosting, in particular, leads to characteristic distortion and "soft lags" in the pulse profiles, which are easily measurable in light curves with moderate energy resolution. With $\sim 10^5$ photons it should also be possible to isolate the more subtle distortions of light travel time variations and frame dragging. Detailed analysis of high quality millisecond pulsar data from upcoming X-ray missions must include these effects.

Subject headings: pulsars: general — X-rays: stars — relativity

1. Introduction

Many neutron star models have thermal surface emission concentrated at magnetic polar caps, which are heated by accretion columns, by precipitating magnetospheric particles, or by anisotropy in the thermal conductivity and heat flow from the interior. A number of authors have computed light curves from such heated polar caps by assuming a stationary dipolar magnetic field and noting that gravitational focusing of the photons can have a substantial effect on the pulse shape (see, e.g. Riffert & Mészáros 1988; Zavlin, Shibanov, & Pavlov 1995). It has also been suggested that resonant scattering on magnetospheric $e^{\pm}$ may modify the thermal light curves (Rajagopal & Romani 1997; Zhu & Ruderman 1997). Recently, pulsed X-ray emission, apparently from the stellar surface, has been detected from a number of very short period neutron stars, including the 5.75ms radio pulsar J0437-4715 (Zavlin & Pavlov 1998) and the 2.49ms LMXB binary J1808.4-3658 (Cui, Morgan, & Titarchuk 1998; Wijnands & van der Klis 1998). For such objects, existing static field and metric approximations may be inadequate.

In this paper we model the effects of rapid rotation on the the surface emission from polar caps. The most prominent effects are associated with simple Doppler boosting at the surface (Ford 1999; Strohmayer et al. 1998). We also model the perturbations associated with the varying time delays of the curved light paths and the pulse distortions resulting from frame-dragging (labeled here as "Kerr") effects on the space-time metric. Previously, Chen & Shaham (1989) noticed the above effects. They modeled the neutron star as a Kerr black hole, and computed values for the star's angular momentum while assuming that the neutron star's surface is stationary in the LNRF (see below). Because of this, they arrive at unphysical values for the angular momentum and only include Doppler shifts due to frame-dragging. We use more realistic values of the frame-dragging angular velocity and include the dominant Doppler boosts caused by the motion of the star's surface in the LNRF. These effects are subtle, but with the increased X-ray sensitivity of *AXAF*, *XMM*, and possibly *USA* careful observations may uncover signatures of rotational perturbations in high statistics energy-resolved light curves of the shortest-period pulsars. The effects will be even more prominent when emission arises from higher altitudes, as is likely for the non-thermal radio and high energy pulsations found in a number of millisecond pulsars (e.g. PSR B1821-24, PSR J0218+4232). Resonant scattering perturbations can also show much larger Doppler and Kerr effects since the flux is re-directed at several R_* and sent back towards the star. Modeling these sources additionally requires a detailed treatment of the retarded (swept-back) B field.

2. The Model

We start by emitting photons from heated polar caps, whose boundary is defined by the last "open" field lines. For this paper we adopt the traditional static field, aligned-rotator estimate of the cap size and use units where $G = c = 1$

$$\sin\theta_{\rm cap} = \sqrt{R_*\Omega_*}, \tag{1}$$

where $\theta_{\rm cap}$ is the half-angular size of the polar cap, R_* is the radius of the star, Ω_* is the angular velocity of the star, Our fiducial model has both caps heated and, for the old, cold neutron stars which have been "recycled", or spun up to short periods, we neglect emission from the rest of the star surface. For a rough approximation, we emit a blackbody spectrum, which will suffer simple interstellar extinction before reaching the observer. The surface emission is assumed to be moderately beamed $I_\nu(\theta_{\rm n}) \propto \cos(\theta_{\rm n})$ to mimic the effect of limb darkening. We have also considered more complicated surface temperature distributions. Fits to real data, seeking to find rapid rotation effects in pulsar light curves, will need to propagate emission from a more realistic thermal spectrum including composition effects, accurate limb darkening, and surface T variation.

The present sums, however, suffice to illustrate the size and characteristic shape of rotation-induced light curve perturbations and will be useful as a guide to when such effects need to be considered.

Formally, our use of Eq. 1 is inconsistent. We have computed the cap distortions induced by the rotational sweep-back of the field lines for a non-aligned dipole (e.g. Deutsch 1955; Romani & Yadigaroglu 1995) including near-surface modifications due to space-time curvature in a Schwarzschild metric (Muslimov & Harding 1997; Prasanna & Gupta 1997; Linet 1975). By generalizing the computation of the field structure of a point dipole in the Schwarzschild metric, we have obtained an expression for a point, rotating dipole in a Schwarzschild space-time that goes to the static Schwarzschild case when $\Omega_* = 0$, goes to the rotating point dipole solution when r gets large, and satisfies Maxwell's equations in the limits $M \to 0$ and $\Omega_* \to 0$, where M is the mass of the pulsar. We can then use this expression to solve for the field lines that are tangent to the light cylinder and define the boundary of the open zone. These lines, when traced back to the surface, result in an irregular shape for the field line foot points and cap boundary. We find that the characteristic cap size is quite close to the simple static estimate for $P \geq 1$ms. After the inclusion of gravitational focusing, the changed cap shape has negligible effect on the light curve; however, when higher altitude emission or scattering are considered, the structure of the relativistic swept-back field is quite important. We defer discussion of these more complex light curves (T.M. Braje & R.W. Romani, in preparation), focusing here on direct surface emission.

Our computation is a Monte Carlo simulation, using the method developed to model resonant scattering perturbations by Rajagopal & Romani (1997). We have extended the photon propagation code to include frame-dragging effects and have modified the transport to follow multiple energy slices of the emitted spectrum, tracing spectral variation through the pulse. We assume a $1.4M_\odot$, 10km ($4.84\mathrm{GM/c^2}$) radius star, and a fiducial spin period $P = 3$ms which gives a cap size of half-angle 15°.

2.1. Boosts

The initial photon directions are drawn in the surface frame with angle θ_n distributed relative to the local normal with probability proportional to $\sin\theta_\mathrm{n}\cos\theta_\mathrm{n}$, and uniformly distributed in ϕ. Although magnetic anisotropies in the surface opacity may break the azimuthal symmetry for higher field pulsars (Pavlov et al. 1994; Rajagopal, Romani, & Miller 1997), this is unlikely to be important for low B, short period neutron stars. These angles give an initial four-momentum of the photon,

$$p^\nu_\mathrm{init} = E_\mathrm{surf}(1, \sin\theta_\mathrm{n}\cos\phi, \sin\theta_\mathrm{n}\sin\phi, \cos\theta_\mathrm{n}). \tag{2}$$

To start the photon trajectories, we must relate a frame co-rotating with the surface of the star, where the photons are emitted with some prescribed spectrum and angular distribution, to a locally Lorentz coordinate frame (Locally Non-Rotating Reference Frame, hereafter the LNRF; e.g., Bardeen, Press, & Teukolsky 1972). The surface velocity of the pulsar, as measured in the

LNRF, is

$$v_{\hat{\phi}} = (\Omega_* - \Omega)\left[\frac{-g_{\phi\phi}}{g_{tt} + \Omega g_{t\phi}}\right]^{\frac{1}{2}} \tag{3}$$

where the stellar angular frequency is Ω_* and the reference frame rotates at $\Omega = -g_{t\phi}/g_{\phi\phi}$. We make a local Lorentz boost to the LNRF

$$p^{\mu}_{\rm final} = \Lambda^{\mu}_{\nu}(v_{\hat{\phi}})p^{\nu}_{\rm init}, \tag{4}$$

choosing the coordinate system so that the y-axis points along the direction of motion, giving

$$\Lambda^{\mu}_{\nu}(v_{\hat{\phi}}) = \begin{pmatrix} \gamma & 0 & -\gamma v_{\hat{\phi}} & 0 \\ 0 & 1 & 0 & 0 \\ -\gamma v_{\hat{\phi}} & 0 & \gamma & 0 \\ 0 & 0 & 0 & 1 \end{pmatrix}. \tag{5}$$

Finally, we convert the photon four-momentum to Boyer-Lindquist coordinates, using the transformations:

$$\begin{aligned} X^{\hat{t}} &= (-g_{tt} - \Omega g_{t\phi})^{1/2}X^{t} \\ X^{\hat{r}} &= (g_{rr})^{1/2}X^{r} \\ X^{\hat{\theta}} &= (g_{\theta\theta})^{1/2}X^{\theta} \\ X^{\hat{\phi}} &= (g_{\phi\phi})^{1/2}[X^{\phi} - \Omega X^{t}] \end{aligned} \tag{6}$$

where X^{μ} represents any four-vector, the left-hand quantities are in the orthonormal LNRF and the right-hand quantities are measured in the Boyer-Lindquist frame.

These initial directions are propagated to large radius $(8R_*)$. The energy boost factor is used to re-weight the surface spectral distribution in the final photon spectrum. We choose a temperature as measured at the surface of the star of 1.3×10^{6}, so that after the Schwarzschild gravitational redshift, the temperature at infinity is 10^{6}K.

2.2. Time Delay

A proper apportionment of photons among final rotational phase (time) bins must include time delay effects arising from both the variation in the curved path length traveled to "infinity" and from the variation in the gravitational time delays experienced by the null geodesics near the star. In practice, we integrate to a fiducial large radius $8R_*$ beyond which flat space propagation, and a constant incremental light travel time, takes us to the observer. The net effect is that the phase coordinate on the two-dimensional sky-map of a photon is corrected by

$$\phi_{\gamma} \rightarrow \phi_{\gamma} - \Omega_* t \tag{7}$$

where t is the (coordinate) time integrated from the surface to the fiducial radius.

This delay will have its strongest effect at the tails of the light curves, where the photons have both traveled the farthest to reach their final destination and spent the most time near the star, suffering bending and time delay in the gravitational field.

2.3. Kerr Propagation

Frame dragging effects around a rotating neutron star will depend on the detailed mass distribution, and hence on the equation of state (EOS) and the spin period. Since neutron stars are moderately centrally condensed and the surface emission starts propagation at $r \geq 3M$, we can adopt a "Roche approximation", assuming all mass is near the origin. This allows us to obtain an approximate set of trajectories by using null geodesics of the Kerr metric. For our chosen pulsar period, mass and radius, we estimate appropriate values for $a(= J/M)$ using the numerical models calculated by Cook, Shapiro, & Teukolsky (1994). We adopt $a = 0.47/P(\mathrm{ms})$ measured in units of M as appropriate to their moderately soft "FPS" model at $M = 1.4M_\odot$ and low R_*. We retain, however, the fiducial 10km radius estimates; note that this is conservative in the sense that Doppler effects at the true $\sim$ 12km radius can be even larger. Note also that $a \propto \Omega_*$ breaks down at $P < 1$ms as the star is rotationally flattened, giving even larger R_* (Cook, Shapiro, & Teukolsky 1994).

Because of certain numerical integration advantages, we use the Kerr metric in a slightly modified form (Rauch & Blandford 1994):

$$\begin{aligned} ds^2 &= -dt^2\left(1-\tfrac{2Mu}{\tilde{\rho}^2}\right)+du^2\tfrac{\tilde{\rho}^2}{u^4(1-2Mu+a^2u^2)}+d\mu^2\tfrac{\tilde{\rho}^2}{u^2(1-\mu^2)} \\ &\quad +d\phi^2\tfrac{(1-\mu^2)(u^{-2}+a^2[\tilde{\rho}^2+\mu^2+2Mu(1-\mu^2)])}{\tilde{\rho}^2}-2d\phi dt\tfrac{2aMu(1-\mu^2)}{\tilde{\rho}^2} \end{aligned} \tag{8}$$

where $\mu = \cos\theta$, $u = r^{-1}$, and $\tilde{\rho}^2 = 1 + a^2\mu^2u^2$. The equations of motion are

$$\begin{aligned} p^t &= \tfrac{dt}{Ed\lambda} = \rho^{-2}\left[-a(a(1-\mu^2)-l)+\tfrac{u^{-2}+a^2}{\Delta}(u^{-2}+a^2-al)\right] \\ p^u &= \tfrac{du}{Ed\lambda} = u_{\mathrm{sgn}}\rho^{-2}\sqrt{1+(a^2-q^2-l^2)u^2+2((a-l)^2+q^2)u^3-a^2q^2u^4} \\ p^\mu &= \tfrac{d\mu}{Ed\lambda} = \mu_{\mathrm{sgn}}\rho^{-2}\sqrt{q^2+(a^2-q^2-l^2)\mu^2-a^2\mu^4} \\ p^\phi &= \tfrac{d\phi}{Ed\lambda} = \rho^{-2}\left[-a+\tfrac{l}{1-\mu^2}+\tfrac{a}{\Delta}(u^{-2}+a^2-al)\right] \end{aligned} \tag{9}$$

where $\rho^2 = u^{-2} + a^2\mu^2$; $\Delta = u^{-2} - 2Mu^{-1} + a^2$; and u_{sgn} and μ_{sgn} are signs that are dependent on the initial direction of the photon. For the initial four-momentum p^ν of our photon in the Boyer-Lindquist frame (Eq. 2), we can compute the constants of motion (l is the z component of angular momentum and q^2 is Carter's constant, both normalized in units of the energy at infinity,

$E = -p_t$) as

$$l = L/E = -p_\phi/p_t \tag{10}$$

$$q^2 = \mathcal{Q}/E^2 = (p_\theta/p_t)^2 + \mu^2[-a^2 + l^2/(1-\mu^2)] \tag{11}$$

where, as usual, $p_\nu = g_{\nu\sigma}p^\sigma$. In order to speed up the computations, we use an elliptic integral reduction of the geodesics presented in Rauch & Blandford (1994).

3. Numerical Results

For our fiducial $\alpha = 60°$, $P = 3$ms case, we have produced high-precision light curves by drawing $\sim 10^8$ photons and mapping the phase distribution in each of 10 energy bands. The computations use simple Schwarzschild propagations (to match the efforts of earlier authors), as well as progressively adding the Doppler boosts, time delays and frame-dragging propagation effects described in Sec. 2.

The results are displayed as sky-maps (Fig. 1) with the intensity of radiation plotted as a function of viewing angle ζ and pulsar phase ϕ. We produce light curves from such images by taking a slice along a particular ζ.

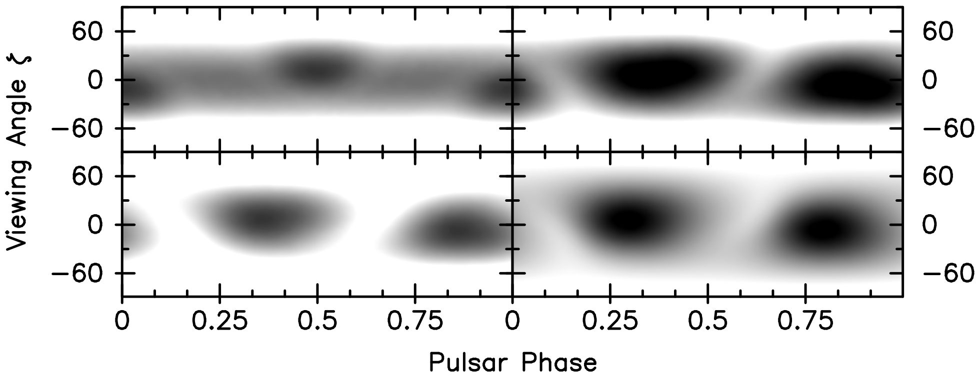

Fig. 1.— All-sky maps of polar cap emission. Parameters: $\alpha = 60°$, $P = 3$ms, two caps of $T_{\rm surf} = 1.3 \times 10^6$ K after interstellar absorption. *Upper Left:* $P \approx 0$ (Schwarzschild), all energies. *Lower Left:* All rotational effects, all energies, shown at the same intensity level as Schwarzschild. *Upper Right:* All effects, low energy band ($0.07 - 0.10$ keV). *Lower Right:* All effects, high energy band ($0.8 - 1.1$ keV). Note the significant distortions and phase shifts.

In Fig. 1, the left panels compare the maps produced by Schwarzschild alone (upper) and the combined rotational effects (lower). Several important differences emerge. In the Schwarzschild map, slightly lighter (fainter) bands border each cap; these are the "shadows" of the opposite pole cast by the star and only partially filled by the facing polar cap. With boosting, time delay and frame dragging, the beam of the cap emission is shifted forward and the simple symmetry around the magnetic axis is broken, so these circular shadows do not appear. The right panels show the variation in the sky-map expected with photon energy. For a $T_{\rm surf} = 1.3 \times 10^6$K, these maps represent the energy bands (at infinity) $0.07 - 0.10$ keV (upper) and $0.8 - 1.1$ keV (lower), respectively. The dramatic enhancement of the hard emission at the leading edge of the pulse is clear, showing the Doppler boost's dominant contribution to the pulse shift.

Simple light curves show more clearly the relative contributions to the pulse shape distortions. Since an observer will only obtain one light curve ($\alpha = 60°$, $\zeta = 80°$ in this case), the effects of the different rotational perturbations can only be isolated by looking at shape distortions, not phase shifts. Accordingly, we shift the light curves by the phase of the best-fitting, two-cycle sinusoid (at $P/2$) to allow direct comparisons (Fig. 2).

As noted by earlier authors, gravitational bending in the Schwarzschild metric greatly decreases the pulse fraction from hot polar caps, by spreading the beam. Also, for stars with two hot caps and masses and radii similar to the fiducial values chosen here, gravitational focusing causes the pulse from one pole to fall in the shadow of the opposite pole, further decreasing the pulse amplitude. Rotational effects break this degeneracy and increase the pulse fraction even for a symmetric two-pole model by a factor of ~ 7 at $P = 3$ms.

The lower panel of Fig. 2 indicates the perturbations in the model light curves (after shifting to the best match sinusoid) which result when the propagation time delay effects are ignored. For $P = 3$ms these produce 8% distortions in the light curve. If "Kerr" propagation effects are ignored the errors are at the 1% level.

The pulse fraction actually decreases in going from the "time delay" case to the "Kerr" case. This effect arises because, in the "Kerr" case, the LNRF has some finite angular velocity with respect to infinity. This angular velocity effectively reduces the initial Doppler boost of the photon from the pulsar's frame to the LNRF. Of course, there is a metric-induced Doppler shift due to the angular velocity of the LNRF (cf. t component of Eq. 6), as noted by Chen & Shaham (1989), but this is a much smaller effect than the true Doppler shift, reducing the pulse fraction of the "Kerr" light curve.

The period dependencies of the pulse-shape distortions are summarized in Fig. 3 and Table 1. We see that even at modest spin frequencies the pulse fraction increases significantly when Doppler boosts are considered. Note that we have assumed a relatively compact star, and surface velocities and Doppler distortions will be even larger for a stiff EOS. For example, using the more realistic radius of $\sim$ 12km for the FPS EOS will increase Doppler boosts by $\sim$ 20%. By $P \sim 3$ms frame dragging and time delay effects are quite substantial. In Table 1 we summarize the pulse fraction (Pulsed counts/Total counts) for Doppler boosted light curves and light curves computed with all rotational effects. These estimates suggest that frame dragging might be measurable below $P \sim 3$ms. In detail, the pulse fractions depend on the ζ chosen, so we have included them for two different viewing angles.

Of course, by using energy cuts we can obtain different weighting of our single line of sight across the pulsar surface. In Fig. 4 we plot normalized light curves in different energy bands for $P = 3$ms. The shifts here are inherently observable since we have absolute phase information of each energy band with respect to the others. Notice that the total shift between the lowest and highest bands is on the order of 15°. In principle, the energy variations allow us to disentangle effects of the Doppler boosting from variations in the underlying star temperature. Sharp spectral features, e.g. absorption lines and edges, will make this task much easier.

4. Discussion and Conclusions

With sufficient count statistics we might hope to isolate the various contributions to the rotational perturbations of the pulsar light curves. To gauge the observational precision required, we simulate data drawn from our model light curves and compare various scenarios. One measure of the significance of the departures is to simulate the data with all rotational effects and to compare with model light curves ignoring either Kerr effects or time delay induced perturbations. For example, for our $P = 3$ms fiducial light curves, we find that pulse profiles depart significantly (95% confidence K-S statistic) from Doppler-alone models when the energy-summed total light curve contains 3×10^4 counts. This does assume a simple model for the surface T distribution (although gravitational focusing renders results surprisingly insensitive to the detailed cap shape). To isolate rotational perturbations in the presence of an arbitrary cap shape and T profile would require significantly more data. Table 1 summarizes the counts required to see Doppler and time-delay/frame-dragging induced distortions for various P.

Intra-band comparisons for a single pulsar are even more robust, since cap shape and T effects will be correlated at the various energies. We have modeled the energy-dependent shape changes. At $P = 3$ms we find that a total of 6×10^4 counts are required to measure the Doppler induced differences between narrow-band lightcurves (10 bands assumed, logarithmically-spaced in energy). For a nearby millisecond pulsar with $T_{\rm cap,surf} = 1.3 \times 10^6$K, $N_H = 10^{19.5}$, we find the most statistically significant differences are typically between the energies (at infinity) less than 0.14 keV and greater than 0.28 keV. These estimates are conservative in that we use only the pulse shape and phase differences. The actual count ratios between energy channels may be used to check the surface T dependence or to allow detection with even lower total counts.

We conclude that high precision models of pulsars such as J0437-4715 must include at least Doppler boosting at the surface. For example Zavlin & Pavlov (1998) have published ROSAT PSPC light curves with good statistics in energy bands extending to $1.1-2.0$ keV with 36° binning. Using model atmospheres and Schwarzschild photon propagation, they have fit for α and ζ, cap size and the detailed T distribution. Our simulations (Fig. 2) suggest that the model light curves (and the parameter values fit) ignoring rotational effects may be substantially in error. For example, fitted M/R_* ratios must be considered preliminary until the effects of rotation are checked. On the other hand the (formally independent) R_* and M dependencies that can be traced to Doppler and gravitational effects suggest that more precise tests of the EOS could be effected with very high quality data and detailed models. High precision *XMM* and *AXAF* data, which are expected, should be suitable for such fitting.

A second example is the newly-discovered 2.49ms accretion-powered pulsar J1808-3658. This source displays strong "soft lags" (Wijnands & van der Klis 1998; Cui, Morgan, & Titarchuk 1998) in the light curves. Ford (1999) has already suggested that this pulsar, as well as a number of QPO sources, exhibits significant Doppler boosting which causes the high energy pulse to lead the softer emission. Alternative explanations, such as Compton down-scatter in a soft corona have been suggested; however, the energy-dependent pulse shape distortions (Cui, Morgan, & Titarchuk 1998) appear very similar to those of Fig. 4. Our computations thus provide significant support for the Doppler boosting interpretation. With more careful modeling it may possible to detect the effect of other rotational distortions to the light curves of this source.

Doppler boosting effects are very significant for these short period thermal cap emitters. Time-delay and frame-dragging distortions, although more subtle, have characteristic shapes that may allow detection. Sources with sharp pulse features, such as the radio and magnetospheric X-ray millisecond pulsars, provide other interesting targets. Resonant Compton scattering can also impart sharp light curve features relatively high in the magnetosphere (Rajagopal & Romani 1997). Doppler effects will, of course, be larger at these altitudes, but significant flux is "lensed" near the star surface in the light curves meaning that the higher-order effects (time-delay and Kerr) may also be significantly enhanced. Modeling of such effects requires detailed treatment of the curved space, swept-back dipole field structure. We will describe such models in a future publication.

This work was supported in part by grants from NASA (NAG 5-3263) and from the Research Corporation. We thank the referee, George Pavlov, for a very careful reading of the manuscript and a number of helpful suggestions.

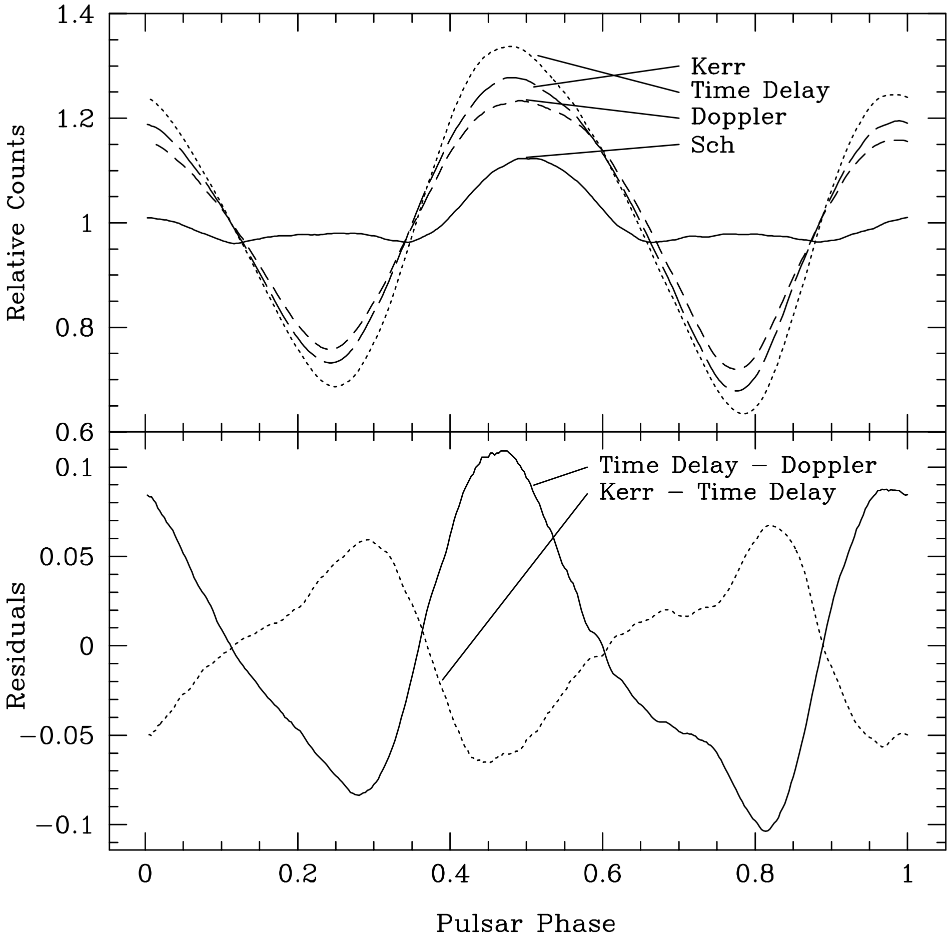

Fig. 2.— Rotational effects on polar light curves (P = 3ms, $\alpha = 60^\circ$, $\zeta = 80^\circ$, cap radius 15°). Curves have been shifted to common phase of a best-fit $P/2$ sinusoid and normalized to a mean count rate per bin of unity. *Above:* Effects of including rotational perturbations. *Below:* Residuals from neglecting time delay or Kerr.

Table 1. Sensitivity to Rapid Rotation Effects.

Statistic	Model	ζ	Sch	12ms	6ms	3ms	1.5ms
Pulse	Dop / Kerr	50°	4.3%	9.6% / 12%	14% / 18%	25% / 30%	34% / 47%
Fraction	Dop / Kerr	80°	4.0%	10% / 12%	15% / 20%	28% / 32%	38% / 53%
N_γ	Energy shift	50°		$\sim 1 \times 10^6$	$\sim 3 \times 10^5$	$\sim 6 \times 10^4$	$\sim 3 \times 10^4$
N_γ	Energy shift	80°		$\sim 2 \times 10^6$	$\sim 4 \times 10^5$	$\sim 6 \times 10^4$	$\sim 4 \times 10^4$
N_γ	Sch *vs.* Dop	50°		$\sim 6 \times 10^4$	$\sim 1 \times 10^4$	$\sim 3 \times 10^3$	$\sim 1 \times 10^3$
N_γ	Sch *vs.* Dop	80°		$\sim 7 \times 10^4$	$\sim 1 \times 10^4$	$\sim 3 \times 10^3$	$\sim 1 \times 10^3$
N_γ	Dop *vs.* Kerr	50°		$\sim 4 \times 10^5$	$\sim 2 \times 10^5$	$\sim 7 \times 10^4$	$\sim 9 \times 10^3$
N_γ	Dop *vs.* Kerr	80°		$\sim 4 \times 10^5$	$\sim 9 \times 10^4$	$\sim 3 \times 10^4$	$\sim 5 \times 10^3$

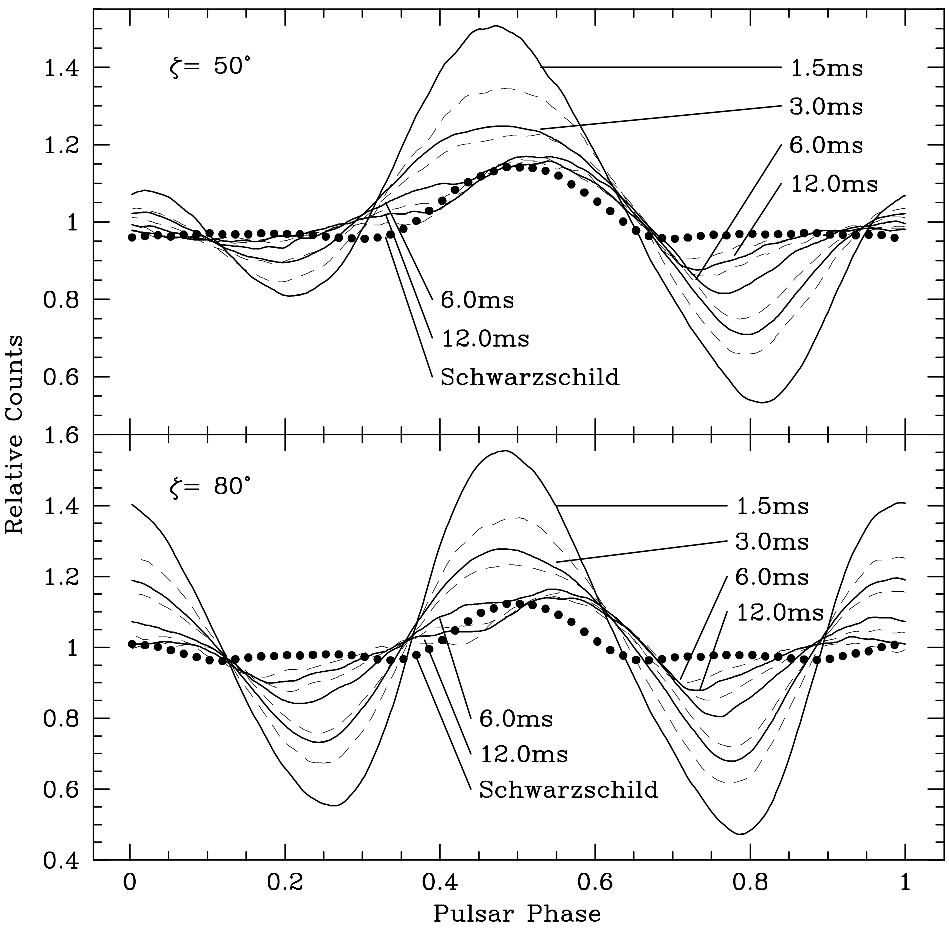

Fig. 3.— Period dependence of light curve distortions ($\alpha = 60°$). Full line: All effects. Dashed line: Doppler boosts only. Points: Reference $P \approx 0$ curve. *Above:* $\zeta = 50°$. *Below:* $\zeta = 80°$.

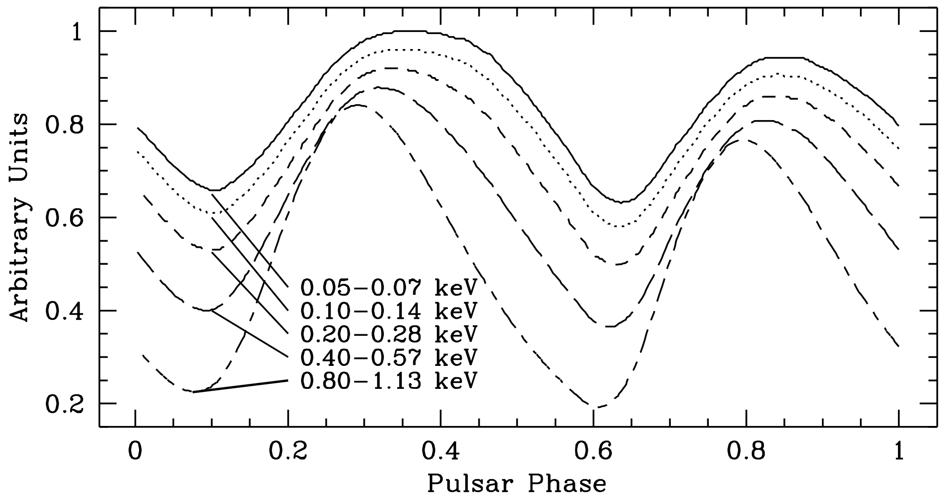

Fig. 4.— Energy dependence on light curve shape, showing Doppler boosting. Arbitrary amplitude normalization.

REFERENCES

Bardeen, J. M., Press, W. H., & Teukolsky, S. A. 1972, ApJ, 178, 347

Chen, K. & Shaham, J. 1989, ApJ, 339, 279

Cook, G. B., Shapiro, S. L., & Teukolsky, S. A. 1994, ApJ, 424, 823

Cui, W., Morgan, E. H., & Titarchuk, L. G. 1998, ApJ, 504, L27

Deutsch, A. J. 1955, Ann. d'Ap., 18, 1

Ford, E. C. 1999, ApJ, 519, 73

Linet, B. 1975, Journal of Physics A, 8, 328

Muslimov, A., & Harding, A. K. 1997, ApJ, 485, 735

Pavlov, G. G., Shibanov, Yu. A., Ventura, J., & Zavlin, V. E. 1994, A&A, 289,837

Prasanna, A. R., & Gupta, A. 1997, Nuovo Cimento B, 112B, 1089

Rajagopal, M., & Romani, R. W. 1997, ApJ, 491, 296

Rajagopal, M., Romani, R. W., & Miller, M. C. 1997, ApJ, 479, 347

Rauch, K. P., & Blandford, R. D. 1994, ApJ, 421, 46

Riffert, H., & Mészáros, P. 1988, ApJ, 325, 207

Romani, R. W., & Yadigaroglu, I.-A. 1995, ApJ, 438,314

Strohmayer, T. E., Zhang, W., Swank, J. H., White, N. E., & Lapidus, I. 1998, ApJ,498,L135

Wijnands, R. & van der Klis, M. 1998, Nature, 394, 344

Zavlin, V. E., & Pavlov, G. G. 1998, A&A, 329, 583

Zavlin, V. E., Shibanov, Yu. A., & Pavlov, G. G. 1995, Astronomy Letters, 21, 149

Zhu, T. & Ruderman, M. 1997, ApJ, 478,701
